

Quantum Ornstein-Zernike Theory for Two-Temperature Two-Component Plasmas

Zachary A. Johnson,^{1,*} Nathaniel R. Shaffer,² and Michael S. Murillo¹

¹*Computational Mathematics, Science and Engineering,
Michigan State University, East Lansing, Michigan 48824, USA*

²*Laboratory for Laser Energetics, University of Rochester,
250 East River Road, Rochester, New York 14623, USA*

(Dated: November 5, 2024)

Laboratory plasma production almost always preferentially heats either the ions or electrons, leading to a two-temperature state. High-fidelity modeling of these systems can be achieved with density functional theory molecular dynamics in the two-temperature, adiabatic electron limit. Motivated by this, we construct a statistical mechanics framework for the multi-temperature system that is theoretically consistent with the *ab initio* calculation. We proceed to derive multi-temperature quantum Ornstein-Zernike equations for the first time. We then construct a two-temperature two-component plasma model using the average atom and compute the radial distribution function, viscosity, ion thermal conductivity, and ion self-diffusion. We verify that we recover the ionic structure and self-diffusion of density functional molecular dynamics simulations.

I. INTRODUCTION

Energy transport and equation of state are crucial physical inputs to accurate modeling of astrophysical environments and terrestrial experiments, including fusion energy efforts. The highly transient nature of inertial fusion energy and laser heated plasma experiments produces plasmas where the electrons and ion species are almost always initially at different temperatures. Hydrodynamic modeling typically takes into account temperature separation [1–3] but the hydrodynamic equations must be closed by calling multi-temperature models for state properties and transport properties.

The current state-of-the-art tool for dense plasma study is density functional theory molecular dynamics (DFT-MD), but typically under the assumption of an equilibrium plasma. However, in principle, it is also capable of modeling two-temperature electron-ion plasmas, and provides a crucial high-fidelity tool for the study of these systems, having been successfully applied to the study of two-temperature plasmas [4–7]. These many-ion calculations are fundamentally limited due to computational expense, making tabulation and experimental fitting difficult when input parameters are uncertain. In the pure equilibrium limit, this niche is filled by the much more rapid average atom (AA) models which provide an all electron but single ion approximation of the DFT-MD calculation. Many iterations of these models exist [8–13], but any that include ion-ion correlations must appeal to the Ornstein-Zernike (OZ) and hypernetted-chain (HNC) equations. These equations are necessary for modeling ionic equation of state contributions, the ion acoustic spectral feature, as well as for electronic and ionic transport coefficients [14, 15].

Previous two-temperature generalizations of the average atom require an ansatz [16, 17] for how the electron and ion temperatures enter into the neutral pseudo atom (NPA) model or require constructing ion-ion potentials by other means such as through Gordon-Kim [18, 19]. In this paper,

we start with the classical weakly coupled limit of Boercker and More, [20], and develop the fully strongly coupled and quantum version, in the form of two-temperature quantum OZ and HNC equations. This provides a rigorous theoretical framework for the generalization of AA models with ions and electrons to the two-temperature limit in a thermodynamically consistent way. In particular, the OZ equations we derive generate an exact form of the two-temperature NPA model of [16] in the adiabatic electron limit, a main result of this paper.

It has been shown that the equilibrium NPA result is in good agreement with equilibrium density functional theory computations [21]. It has additionally been used to calculate non-equilibrium equation of state [22], acoustic modes [23], and electronic transport [24], but has not been similarly validated against explicit two-temperature DFT-MD calculations as in the equilibrium case. We take the AA model in [10], and show how it and other AA models can be generalized to the two-temperature limit as in the NPA model, to generate a two-temperature two-component plasma (2TTCP) model. We then compare it against radial distribution functions and self-diffusion with two-temperature *ab initio* DFT-MD simulation, finding excellent agreement. We further compute the ion thermal conductivity and ion viscosity from molecular dynamics, comparing against the results of [19]. We also determine the reliability of on-the-fly ionic transport coefficient models in the two-temperature limit [25–27]. The validation of the 2TTCP approach as a generalization of equilibrium AA models against DFT-MD, and the production of non-equilibrium ionic transport coefficients are the other main results of this paper.

In section II we introduce our multi-temperature partition function and the accompanying thermodynamic framework. We then derive the two temperature quantum Ornstein-Zernike (QOZ) and hypernetted-chain (HNC) equations. In section III we use these ideas to create a two-temperature, two-component plasma model based on the average atom. We then compute ionic transport coefficients, and radial distribution functions, comparing results with the literature.

* john8248@msu.edu

II. MULTIPLE TEMPERATURE STATISTICAL MECHANICS

Materials with multiple temperatures are by definition out of local thermal equilibrium (LTE), and yet if a hierarchy of timescales is involved, then an approximate equilibrium to develop, which can thus be described by a partition function. In the case of an electron-ion plasma, this hierarchy is $\tau_{ee} < \tau_{II} < \tau_{eI}$ where τ_{ij} is the thermodynamic relaxation time between species i, j . We denote electrons and ions by e, I , respectively. This leads to an adiabatic electron description used for example in the DFT-MD codes[28–30]. The electrons in this picture relax in a fixed external potential, under the Hamiltonian

$$\begin{aligned} \hat{H}_e &= H_{ee} + H_{eI} \\ &= -\frac{1}{2} \sum_i \hat{p}_i^2 + \frac{1}{2} \sum_{i \neq j} \frac{1}{|\hat{\mathbf{r}}_i - \hat{\mathbf{r}}_j|} - \sum_i V_i^{\text{ext}}(\{\mathbf{r}_I\}) \end{aligned} \quad (1)$$

This is a function of all ion coordinates r_I . Instead of the explicit external potential from the ions, we will instead frequently call,

$$\hat{\psi}_e = \mu_e - \hat{V}_e^{\text{ext}}(\{\mathbf{r}_I\}), \quad (2)$$

the external potential. This specifies the partition function for the electrons,

$$\begin{aligned} \Xi_e &= \exp\{-\beta_e \Omega_e\} \\ &= \sum_{N_e} \text{Tr} e^{-\beta_e (\hat{H}_{ee} - \sum_i \hat{\psi}_{ei} - \mu_e \hat{N}_e)}. \end{aligned} \quad (3)$$

with electron inverse temperature β_e , grand potential Ω_e . For each ion configuration, the electrons are assumed to minimize this potential,

$$\frac{\delta \Omega_e(\{\mathbf{r}_I\})}{\delta n_e} = 0 \quad (4)$$

This fixes the electronic physics, but the more nontrivial step is determining the statistical mechanics of the ions in the presence of these electrons. The ion-ion Hamiltonian itself is

$$H_{II} = \sum_i \frac{\mathbf{p}_i^2}{2m_I} + \sum_{i \neq j} \frac{1}{2} \frac{Z_I^2}{|\mathbf{r}_i - \mathbf{r}_j|}, \quad (5)$$

Since the electrons minimize the grand energy for constant temperature and chemical potential, it is the grand energy which affects the forces and energetics of the ion subsystem, giving

$$\Xi = \sum_{N_I} \int \prod_i^{N_I} \frac{d^3 \mathbf{r}_i d^3 \mathbf{p}_i}{(2\pi\hbar)^{3N_I}} e^{-\beta_I (H_{II} + \Omega_e - \sum_i \psi_I(\mathbf{r}_i))}, \quad (6)$$

where N_I is the total ion number for a given ensemble and we refer to $\psi_I(\mathbf{r}_i) = \mu_I - V_I^{\text{ext}}$ as the external potential as in Eq. (2). This idea is essentially the ansatz of [20] where it was applied to study classical, weakly interacting particles. In App. A we present a statistical derivation of

this partition function and increase the connection with DFT-MD simulations.

$$\Omega = -T_I \ln \Xi. \quad (7)$$

From the grand potential we also have a free energy, F corresponding to generalization of the Helmholtz free energy to two-temperature systems. These are related via

$$\Omega = F - \sum_j^N \mu_j \int d^3 \mathbf{r} n_j, \quad (8)$$

where μ_j is the chemical potential and n_j is the number density of species j . Each species will have its own external potential V_j^{ext} . A more useful object here is the intrinsic free energy, which in an abuse of notation, we will simply refer to as the free energy,

$$\mathcal{F} = F - \sum_j^N \int d^3 \mathbf{r} V_j^{\text{ext}} n_j. \quad (9)$$

This is the Legendre transform of the free energy with respect to ψ_j ,

$$\Omega = \mathcal{F} - \int d^3 \mathbf{r} n \psi. \quad (10)$$

The free energy is additionally split into the ideal, or free, and excess components in the standard way[31] as

$$\mathcal{F} = \mathcal{F}^{\text{id}} + \mathcal{F}^{\text{ex}}. \quad (11)$$

We proceed by defining the response function and the polarization potential, respectively, as

$$\frac{\delta^2 \Omega}{\delta \psi_i(\mathbf{r}) \delta \psi_j(\mathbf{r}')} = -\frac{\delta n_i(\mathbf{r})}{\delta \psi_j(\mathbf{r}')} \equiv \chi_{ij}(\mathbf{r}, \mathbf{r}'), \quad (12)$$

$$\frac{\delta^2 \mathcal{F}^{\text{ex}}[\{n\}]}{\delta n_i(\mathbf{r}) \delta n_j(\mathbf{r}')} = \frac{\delta \psi_i(\mathbf{r})}{\delta n_j(\mathbf{r}')} + \chi_{ij}^0{}^{-1}(\mathbf{r}, \mathbf{r}') \equiv U_{ij}(\mathbf{r}, \mathbf{r}'). \quad (13)$$

In fully equilibrated systems the polarization potential U_{ij} , is related to the direct correlation function as $c_{ij} = -\beta U_{ij}$. Working with the polarization potential instead allows us to remain agnostic about the nature of β when $T_I \neq T_J$. Constructing the Ornstein-Zernike equation begins with the definition of the functional inverse,

$$\sum_k \int \chi_{ik}(\mathbf{r}, \mathbf{r}'') \chi_{ki}^{-1}(\mathbf{r}'', \mathbf{r}') d\mathbf{r}'' = \delta_{ij} \delta(\mathbf{r} - \mathbf{r}'). \quad (14)$$

For homogeneous systems, we write this in k-space and as a matrix equation over species space, giving us the Dyson equation for the response function,

$$\boldsymbol{\chi}(k) = (\boldsymbol{\chi}_0^{-1}(k) - \mathbf{U}(k))^{-1}. \quad (15)$$

Given the theoretical importance of electron-ion plasma, it is instructive to consider the specific case of a two species plasma, for which we have,

$$\chi = \frac{1}{D} \begin{pmatrix} \chi_{011}(1 - \chi_{022} U_{22}) & \chi_{011} \chi_{022} U_{12} \\ \chi_{011} \chi_{022} U_{12} & \chi_{022}(1 - \chi_{011} U_{11}) \end{pmatrix}. \quad (16)$$

and the determinant is,

$$D = (1 - \chi_{022} U_{22})(1 - \chi_{011} U_{11}) - \chi_{011} \chi_{022} U_{12}^2. \quad (17)$$

This reduces to the equilibrium answer[32] when $U_{ij} \rightarrow \beta_i c_{ij}$.

A. Two-Temperature Quantum Ornstein-Zernike Relations

Now that we have the partition function for our system, we can produce plasma correlation functions. From Eq. (10) we have

$$\frac{\delta\Omega}{\delta\psi_j(\mathbf{r})} = -n_j(\mathbf{r}), \quad (18)$$

but it is instructive to obtain this again from the partition function. For the ion, the result is the standard result

$$\begin{aligned} \frac{\delta\Omega}{\delta\psi_I(\mathbf{r})} &= -\frac{1}{\Xi} \text{Tr}_I \left[\sum_k \delta^3(\mathbf{r} - \mathbf{r}_k) \right], \\ &= -\langle \hat{n}_I \rangle, \\ &\equiv -n_I(\mathbf{r}) \end{aligned} \quad (19)$$

For the electron, we have two possible electron densities, one with a specific ion configuration, and another averaged over all ion configurations. Thus, we have

$$\begin{aligned} \frac{\delta\Omega}{\delta\psi_e(\mathbf{r})} &= -\frac{1}{\Xi} \text{Tr}_I \left[\frac{\delta\Omega_e[\{\mathbf{r}_I\}]}{\delta\psi_e(\mathbf{r})} \right], \\ &= -\frac{1}{\Xi} \text{Tr}_I \left[-\frac{1}{\Xi_e} \text{Tr}_e [\hat{n}_e](\{\mathbf{r}_I\}) \right], \\ &= -\text{Tr}_I [n_e(\{\mathbf{r}_I\})], \\ &\equiv -n_e(\mathbf{r}). \end{aligned} \quad (20)$$

as expected. The second functional derivative generates the density-density correlation functions through

$$\frac{\delta^2\Omega}{\delta\psi_i(\mathbf{r}')\delta\psi_j(\mathbf{r})} = -\frac{1}{\beta_I\Xi} \frac{\delta^2\Xi}{\delta\psi_i(\mathbf{r}')\delta\psi_j(\mathbf{r})} + \frac{1}{\beta_I} \frac{\delta \ln \Xi}{\delta\psi_i(\mathbf{r}')} \frac{\delta \ln \Xi}{\delta\psi_j(\mathbf{r})}. \quad (21)$$

The ion-ion term is [31],

$$\begin{aligned} \frac{\delta^2\Omega}{\delta\psi_I(\mathbf{r}')\delta\psi_I(\mathbf{r})} &= -\beta_I \langle \hat{n}_I(\mathbf{r})\hat{n}_I(\mathbf{r}') \rangle_I - \beta_I n_I(\mathbf{r})n_I(\mathbf{r}'), \\ &\equiv -\beta_I H_{II}(\mathbf{r}, \mathbf{r}'), \end{aligned} \quad (22)$$

Where H_{ij} describes fluctuations in the density-density correlation about the background,

$$H_{II}(\mathbf{r}, \mathbf{r}') = \langle (\hat{n}_I(\mathbf{r}) - \langle \hat{n}_I(\mathbf{r}) \rangle_I) (\hat{n}_I(\mathbf{r}') - \langle \hat{n}_I(\mathbf{r}') \rangle_I) \rangle_I. \quad (23)$$

The ion-electron term is likewise

$$\begin{aligned} \frac{\delta^2\Omega}{\delta\psi_i(\mathbf{r}')\delta\psi_e(\mathbf{r})} &= -\beta_I \langle \hat{n}_I(\mathbf{r}') \frac{\delta\Omega_e[\{\mathbf{r}_I\}]}{\delta\psi_e(\mathbf{r})} \rangle_I + \beta_I n_I(\mathbf{r}')n_e(\mathbf{r}), \\ &\equiv -\beta_I H_{Ie}(\mathbf{r}, \mathbf{r}'), \end{aligned} \quad (24)$$

where one can check explicitly that the commuted functional derivatives give the same result, and

$$H_{Ie}(\mathbf{r}, \mathbf{r}') = \langle (\hat{n}_I(\mathbf{r}) - \langle \hat{n}_I(\mathbf{r}) \rangle_I) (n_e(\{\mathbf{r}_I\}) - \langle n_e(\{\mathbf{r}_I\}) \rangle_I) \rangle_I. \quad (25)$$

The electron-electron term is additionally complicated by the need for a chain rule operation on the exponential of the electron grand potential, resulting in

$$\begin{aligned} \frac{\delta^2\Omega}{\delta\psi_e(\mathbf{r}')\delta\psi_e(\mathbf{r})} &= \left\langle \frac{\delta^2\Omega_e[\{\mathbf{r}_I\}]}{\delta\psi_e(\mathbf{r}')\delta\psi_e(\mathbf{r})} - \beta_i \frac{\delta\Omega_e[\{\mathbf{r}_I\}]}{\delta\psi_e(\mathbf{r})} \frac{\delta\Omega_e[\{\mathbf{r}_I\}]}{\delta\psi_e(\mathbf{r}')} \right\rangle_I \\ &\quad + \beta_I n_e(\mathbf{r}')n_e(\mathbf{r}). \end{aligned} \quad (26)$$

This first term in Eq. (26) is the density-density fluctuation term in a specific fixed ion configuration,

$$\frac{\delta^2\Omega_e[\{\mathbf{r}_I\}]}{\delta\psi_e(\mathbf{r}')\delta\psi_e(\mathbf{r})} = -\beta_e H_{ee}(\mathbf{r}, \mathbf{r}'; \{\mathbf{r}_I\}). \quad (27)$$

which is,

$$H_{ee}(\mathbf{r}, \mathbf{r}'; \{\mathbf{r}_I\}) = \langle \hat{n}_e(\mathbf{r})\hat{n}_e(\mathbf{r}') \rangle_e - n_e(\mathbf{r}; \{\mathbf{r}_I\})n_e(\mathbf{r}'; \{\mathbf{r}_I\}). \quad (28)$$

Inserting this into Eq. (26) gives

$$\begin{aligned} \frac{\delta^2\Omega}{\delta\psi_e(\mathbf{r}')\delta\psi_e(\mathbf{r})} &= -\beta_e \langle \hat{n}_e(\mathbf{r})\hat{n}_e(\mathbf{r}') \rangle_{e,I} \\ &\quad + (\beta_e - \beta_I) \langle n_e(\mathbf{r}; \{\mathbf{r}_I\})n_e(\mathbf{r}'; \{\mathbf{r}_I\}) \rangle_I \\ &\quad + \beta_I n_e(\mathbf{r}')n_e(\mathbf{r}). \end{aligned} \quad (29)$$

The second term on the right hand side is a newly relevant correlation function, being the ion-averaged correlation between one-body electron densities. It is a perfectly well-defined function even in the equal temperature limit, but never enters.

To accommodate this new correlation structure, we define another electron-electron density-density fluctuation function,

$$H_{ee}(\mathbf{r}, \mathbf{r}') = \langle \hat{n}_e(\mathbf{r})\hat{n}_e(\mathbf{r}') \rangle_e - n_e(\mathbf{r})n_e(\mathbf{r}'), \quad (30)$$

which is distinct from Eq. (28) in that the one-body densities have been averaged over ion configurations independently.

We have the difference,

$$\begin{aligned} \Delta H_{ee}(\mathbf{r}, \mathbf{r}') &= H_{ee}(\mathbf{r}, \mathbf{r}') - \langle H_{ee}(\mathbf{r}, \mathbf{r}'; \{\mathbf{r}_I\}) \rangle_I \\ &= \langle n_e(\mathbf{r}; \{\mathbf{r}_I\})n_e(\mathbf{r}'; \{\mathbf{r}_I\}) \rangle_I - n_e(\mathbf{r})n_e(\mathbf{r}'). \end{aligned} \quad (31)$$

This implies

$$\frac{\delta^2\Omega}{\delta\psi_e(\mathbf{r}')\delta\psi_e(\mathbf{r})} = -\beta_e H_{ee}(\mathbf{r}, \mathbf{r}') + (\beta_e - \beta_I) \Delta H_{ee}(\mathbf{r}, \mathbf{r}') \quad (32)$$

This non-equilibrium correction to the electron-electron behaviour can be easily thought of in two extreme limits, the homogeneous electron gas (HEG), and the tight-binding limit. In the first case, the ions are spread homogeneously in space, so the one-body density is likewise homogeneous and the β_I dependence cancels exactly. In the opposite limit of tight-binding electrons (TB), the electron number density is essentially composed of delta functions around the ions, and ion-ion correlations enter, as in

$$\begin{aligned}\Delta H_{ee}(\mathbf{r}, \mathbf{r}') &\xrightarrow{\text{HEG}} 0 \\ \Delta H_{ee}(\mathbf{r}, \mathbf{r}') &\xrightarrow{\text{TB}} Z^2 H_{II}(\mathbf{r}, \mathbf{r}').\end{aligned}$$

We can also see that in the very cold ion limit, the ion-correlations become dominant. These fluctuations are connected to the response function via Eq. (12), giving

$$\chi_{II}(\mathbf{r}, \mathbf{r}') = -\beta_I H_{II}(\mathbf{r}, \mathbf{r}') \quad (33a)$$

$$\chi_{Ie}(\mathbf{r}, \mathbf{r}') = -\beta_I H_{Ie}(\mathbf{r}, \mathbf{r}') \quad (33b)$$

$$\chi_{eI}(\mathbf{r}, \mathbf{r}') = -\beta_I H_{Ie}(\mathbf{r}, \mathbf{r}') \quad (33c)$$

$$\chi_{ee}(\mathbf{r}, \mathbf{r}') = -\beta_e H_{ee}(\mathbf{r}, \mathbf{r}') + (\beta_e - \beta_I) \Delta H_{ee}(\mathbf{r}, \mathbf{r}'). \quad (33d)$$

We now construct a form of the Ornstein-Zernike relations in terms of the polarization potential U_{ij} in Eq. (13), and the dimensionless pair correlation function,

$$h_{ij}(\mathbf{r}, \mathbf{r}') = \frac{H_{ij}(\mathbf{r}, \mathbf{r}')}{n_i(\mathbf{r})n_j(\mathbf{r}')} - \frac{\delta_{ij}\delta_{ij}(\mathbf{r} - \mathbf{r}')}{n_i(\mathbf{r})}, \quad (34)$$

as well as the dimensionless electron-electron deviation from the HEG limit

$$\Delta h_{ee}(\mathbf{r}, \mathbf{r}') = \frac{\Delta H_{ee}(\mathbf{r}, \mathbf{r}')}{n_e(\mathbf{r})n_e(\mathbf{r}')} - 1 \quad (35)$$

We now take the classical ion limit, $\chi_{11}^0 = -\beta_i n_i$, and assume homogeneity. In Fourier space, from Eq. (16) we get,

$$\tilde{h}_{II}(k) = -\frac{1}{D}\beta_i(U_{II} - \chi_{0ee}(U_{II}U_{ee} - U_{eI}^2)) \quad (36a)$$

$$\tilde{h}_{Ie}(k) = \frac{1}{D}n_e^{-1}\chi_{0ee}U_{Ie} \quad (36b)$$

$$\tilde{h}_{eI}(k) = \frac{1}{D}n_e^{-1}\chi_{0ee}U_{eI} \quad (36c)$$

$$\begin{aligned}\tilde{h}_{ee}(k) &= (1 - \beta_I/\beta_e)\widetilde{\Delta h}_{ee} - n_e^{-1}(1 + n_I\beta_I\tilde{U}_{II})(1 + \frac{\chi_{ee}^0}{\beta_e n_e}) \\ &\quad \frac{1}{D}n_e^{-1}\chi_{0ee}(U_{ee} + n_I\beta_I(U_{II}U_{ee} - U_{eI}^2)).\end{aligned} \quad (36d)$$

These are the two-temperature generalizations of the quantum Ornstein-Zernike relation and is a major result of this paper. To see another way in which they can be written, consults App. C. One can see that in the equilibrium limit $\beta_I = \beta_e$ the new correlation term $\widetilde{\Delta h}_{ee}$ drops out, and taking the classical limit for the electrons makes it symmetric with the ions. One can then recover the equilibrium OZ relations via $U_{ij} \rightarrow \beta c_{ij}$.

B. Hypernetted-Chain for Two-Temperature Systems

We have connected the response function to spatial correlation functions, but as of yet we require a closure that connects the polarization potential to these functions. In a classical equilibrium system, this is typically in the form of the hypernetted chain closure, with or without corrections[33–35]. In many two-temperature papers

[20, 36, 37] this closure is commonly referenced, but a derivation has never been given to our knowledge, nor is it obvious what the multi-temperature generalization of the direct correlation function c_{ij} is supposed to be. It would seem particularly troubling since the canonical form of the HNC approximation,

$$h_{ij} + 1 = e^{-\beta u_{ij} + h_{ij} - c_{ij}} \quad (37)$$

implicitly incorporates the Ornstein-Zernike relations[31], which were modified in [36, 37].

In this section, we derive the multi-temperature generalization of Eq. (37). One can derive an exact second order the multiple temperature extension via coupling constant integration of the free energy over a density from a uniform system to an inhomogeneous system[31], but it is far more practical to approximate with the polarization potential in the homogeneous limit, which defines the HNC approximation. To do this we take a second order Taylor expansion of the free energy in terms of the density,

$$n_i(\mathbf{r}) = n_{0i} + \Delta n_i(\mathbf{r}). \quad (38)$$

In terms of the polarization potential Eq. (13), we have

$$\begin{aligned}\mathcal{F}^{\text{ex}}[\{n\}] &= \mathcal{F}^{\text{ex}}[\{n_0\}] + \sum_i \mu^{\text{ex}} \int d\mathbf{r} \Delta n_i(\mathbf{r}) \\ &\quad + \frac{1}{2} \sum_{ij} \int d\mathbf{r} d\mathbf{r}' U_{ij}(\mathbf{r}, \mathbf{r}') \Delta n_i(\mathbf{r}) \Delta n_j(\mathbf{r}') + \sum_{ij} B_{ij}\end{aligned} \quad (39)$$

Where we use the excess chemical potential $\mu^{\text{ex}} = \frac{\delta \mathcal{F}^{\text{ex}}[n_0]}{\delta n_i} = \psi - \frac{\delta \mathcal{F}^{\text{id}}[n_0]}{\delta n_i} = \mu - \frac{\delta \mathcal{F}^{\text{id}}[n_0]}{\delta n_i}$, and the bridge function, B_{ij} , encodes the difference between the homogeneous polarization potential and the exact heterogeneous polarization potential one could obtain from a coupling constant integration. Here we can see the advantage of using the polarization potentials rather than the direct correlation functions as we as of yet do not have to specify any temperatures.

Inserting this expression into grand energy Eq. (10), the Euler equation we get is,

$$0 = \frac{\delta \Omega}{\delta n_i(r)} \quad (40)$$

$$\begin{aligned}&= \frac{\delta \mathcal{F}^{\text{id}}[n_i]}{\delta n_i(r)} + \mu^{\text{ex}} - \psi_i(\mathbf{r}) \\ &\quad + \sum_j \int d\mathbf{r}' U_{ij}(\mathbf{r}, \mathbf{r}') \Delta n_j(\mathbf{r}') + \sum_j \frac{\delta B_{ij}}{\delta n_i(r)}\end{aligned} \quad (41)$$

The discussion thus far is general to quantum and classical systems, but now the electrons and ions must be separately handled. In the classical limit, for the ions, we have

$$0 = T_i \ln(n_i(\mathbf{r})/n_0(\mathbf{r})) + \sum_j \int d\mathbf{r}' U_{ij}(\mathbf{r}, \mathbf{r}') \Delta n_j(\mathbf{r}') + \quad (42)$$

$$\phi(\mathbf{r}) + \sum_j \frac{\delta B_{ij}}{\delta n_i(r)}. \quad (43)$$

For the electrons, we instead take the Kohn-Sham picture and create a non-interacting system in a modified effective potential[38]

$$\phi_i^{\text{eff}}(\mathbf{r}) = \phi_i(\mathbf{r}) + \sum_j \int d\mathbf{r}' U_{ij}(\mathbf{r}, \mathbf{r}') \Delta n_j(\mathbf{r}'), \quad (44)$$

with a chemical potential $\mu_i^0 = \mu_i + \mu_i^{\text{ex}}$. To connect this density with correlation functions we use Percus's trick, $n_i(\mathbf{r}; \phi) = n_i g_{ij}^{(2)}(\mathbf{r}, \mathbf{r}'; \phi = 0)$, where ϕ represents an external potential from fixing particle j at \mathbf{r}' . It is only possible to fix classical particles at the origin in this way, but the number density can be for any species. This allows us to obtain g_{ei} , g_{II} , but not g_{ee} , whose closure is unknown. We note for the reader interested in purely classical systems, that even here Percus's trick is highly non-trivial for the lighter species.

With the ion so fixed at the origin, we obtain

$$g_{II}(\mathbf{r}) = \exp \left[-\beta_i u_{II}(\mathbf{r}) - \sum_{j=e,I} n_j \int d\mathbf{r}' \beta_I U_{Ij}(\mathbf{r}, \mathbf{r}') h_{jI}(\mathbf{r}') \right], \quad (45a)$$

$$g_{eI}(\mathbf{r}) = n_e^{-1} n_e \left(\mathbf{r} | u_{eI}(\mathbf{r}) + \sum_{j=e,I} n_j \int d\mathbf{r}' U_{ej}(\mathbf{r}, \mathbf{r}') h_{jI}(\mathbf{r}') \right). \quad (45b)$$

The ion-ion equation can be simplified even further through a rewritten form of the QOZ equations Eq. (C2a), to obtain

$$g_{II}(\mathbf{r}) = \exp[-\beta_I u_{II}(\mathbf{r}) + h_{II} + \beta_I U_{II}]. \quad (46)$$

This is remarkably the exact standard form of the HNC approximation if one replaces $\beta_I U_{II}$ with $-c_{II}$, which is likely why models such as [37] are so successful in the classical limit, despite not ever deriving a generalized HNC. The electron-ion term also simplifies using Eq. (C2b)

$$g_{eI}(\mathbf{r}) = n_e^{-1} n_e (\mathbf{r} | u_{eI}(\mathbf{r}) - U_{eI}(\mathbf{r}) + h_{eI}(\mathbf{r}) n_e \chi_{0ee}^{-1}). \quad (47)$$

We will see in the next section that our final results do not use Eq. (47), due to the computational difficulty of such a self-consistent picture and the fact that this approximation neglects bridge functions which are likely quite large for all electron computations.

III. TWO-TEMPERATURE TWO-COMPONENT PLASMA MODEL

The combination of the QOZ equations, Eq. (36) and the HNC approximation Eq. (45) make a consistent theory that can be solved once electron-electron information is incorporated through, for instance, a HEG model. The single temperature consistent calculation would then be similar to [11, 38]. We instead model the electron-ion polarization potential as a linear-response pseudopotential to avoid issues with the unknown bridge function, via

$$\tilde{U}_{ei}(k) \approx \frac{\tilde{n}_e^{sc}(k)}{\tilde{\chi}_{ee}(k)}. \quad (48)$$

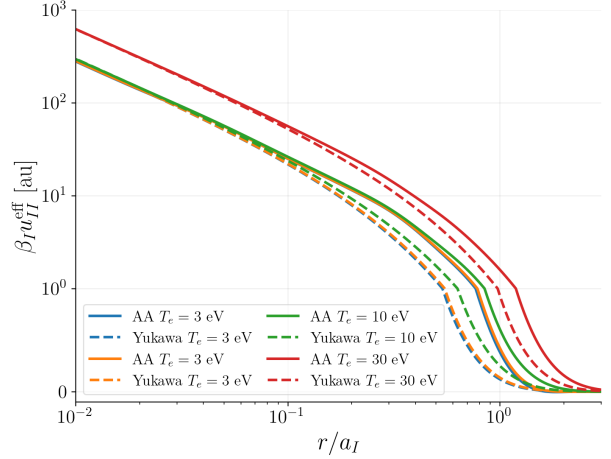


FIG. 1. The AA produced pair potential 52 (solid lines), and Yukawa pair potential (dashed) with Thomas-Fermi screening using a $\langle Z \rangle$ from the AA model. Higher electron temperatures are right most.

Where n_e^{sc} is the electron screening density as defined in [10]. This loses what is effectively the electron-ion local-field correction that relates the potential and the polarization potential, and we work additionally in a non-self consistent picture where the average atom computation is done with a fixed empty-core ion distribution function. The motivation is that this is a drastic computational simplification, still rigorously incorporates the multi-temperature QOZ equations, albeit approximately, is known to be very close to the self-consistent answer in many cases[10].

We construct our two-temperature two-component plasma model (2TTCP) from the AA via using the QOZ equations to generate the exact effective single particle interaction. From Eq. (36), we have

$$h_{II}(\mathbf{r}, \mathbf{r}') = -\frac{\beta_I U_{II} - \beta_I \chi_{0ee} (U_{II} U_{ee} - U_{eI}^2)}{(1 - \chi_{0ee} U_{ee})(1 + n_I \beta_I U_{II}) + n_I \beta_I \chi_{0ee} U_{eI}^2}. \quad (49)$$

This can be rewritten as an effective single-species problem,

$$h_{II}(\mathbf{r}, \mathbf{r}') = -\frac{\beta_I U_{II}^{\text{eff}}}{1 + n_I \beta_I U_{II}^{\text{eff}}} \quad (50)$$

using the effective polarization potential,

$$U_{II}^{\text{eff}} = U_{II} + \frac{\chi_{ee}^0}{1 - \chi_{ee}^0 U_{ee}} U_{ei}^2. \quad (51)$$

Note that this is exact within the ion-ion HNC approximation, meaning deviations are only possible through at most a bridge function, and does not require a Taylor expansion. This effective potential is,

$$\begin{aligned} u_{II}^{\text{eff}} &= u_{II} - U_{II} + U_{II}^{\text{eff}} \\ &= \phi_{II} + \frac{\chi_{ee}^0}{1 - \chi_{ee}^0 U_{ee}} U_{ei}^2. \end{aligned} \quad (52)$$

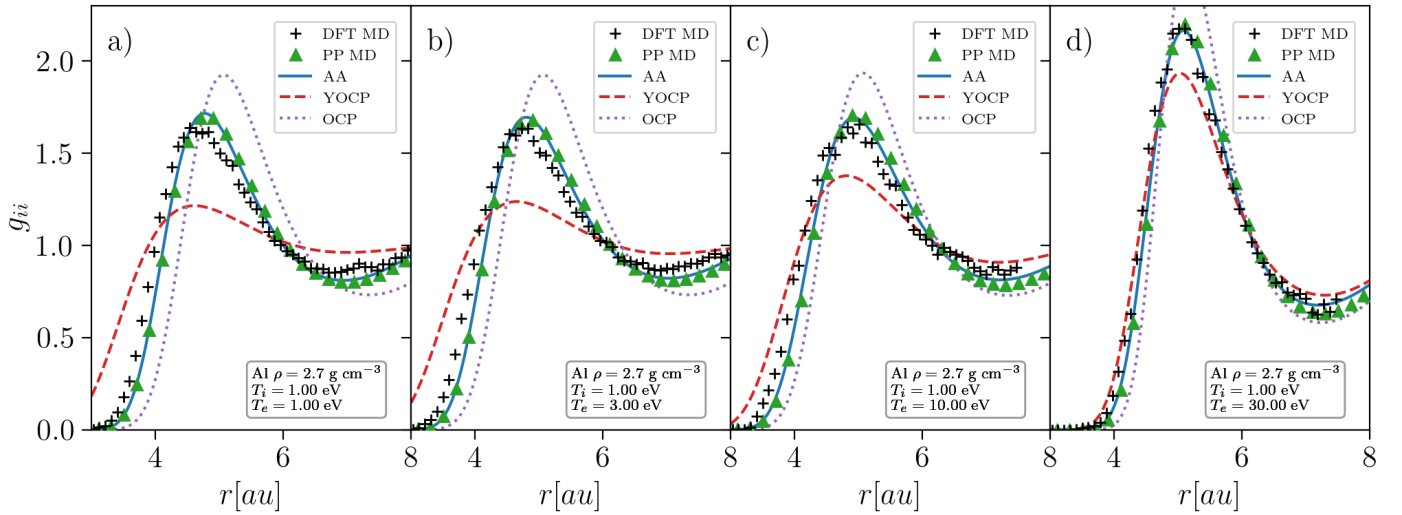


FIG. 2. Ion-ion radial distribution function for Aluminum at solid density 2.7g/cm^4 and fixed $T_I = 1\text{ eV}$, with increasing electron temperature from left to right, **a)** LTE: $T_e = 1\text{ eV}$ ($\langle Z \rangle = 3.00$), **b)** $T_e = 3\text{ eV}$ ($\langle Z \rangle = 3.00$), **c)** $T_e = 10\text{ eV}$ ($\langle Z \rangle = 3.02$), **d)** $T_e = 30\text{ eV}$ ($\langle Z \rangle = 4.35$). We show DFT-MD (black plus), classical MD with our 2TTCP pair potential, and HNC with bridge function computations for the 2TTCP (blue solid), the YOCP (red dashed), and the OCP (purple dotted).

Using any AA model, one can use Eq. (48) to create the approximate electron-ion polarization potential to complete the effective potential. This then generates the ionic structure of the plasma in the form of h_{II} , or $S_{II}(k)$. We note importantly that this equation for the effective potential has been used by Dharma-Wardana in, for instance, [16]. The 2TTCP model presented here is thus a similar extension of the NPA model but for the AA model of [10]. Neither of these models fully incorporates the self-consistent set of QOZ/HNC equations, which we leave to later study. We note that there was discussion [39] on the validity of results based on the two temperature NPA. This motivated us to very carefully benchmark our model against DFT-MD explicitly, which we show below.

A. Plasma Structure

The electron and ion temperature are different levers on the structural and transport properties of dense plasmas. We investigate these effects through the 2TTCP model defined above, and compare to ab initio DFT-MD and on-the-fly transport models when possible.

The effect of the electron temperature on the ions can be seen readily from the 2TTCP pair potential, Eq. (52). In the case of a simple metal like aluminum with well defined bound and valence states, T_e variations largely only impact ionic properties through ionization, which occurs at $\gtrsim 10\text{ eV}$. In Fig. 1 we can see both the effects of this ionization through the difference between the cooler (green, orange, blue) lines and the $T_e = 30\text{ eV}$ lines (red) as well as the importance of the non-linear screening in the 2TTCP (solid lines) versus the Yukawa one component plasma (YOCP) model (dashed lines).

We benchmark the accuracy of our 2TTCP model with DFT-MD simulations from VASP [29, 40, 41] with an

11 electron projector augmented wave pseudopotential[42]. The 11 electron pseudopotential electron was necessary to capture ionization. For the $T_e = 1, 3\text{ eV}$ cases, we use 64 atoms, and for the $T_e = 10, 30\text{ eV}$ cases, we use 32 atoms.

We also run ion-ion pair potential MD using LAMMPS[43] and the 2TTCP pair potential (PPMD). We use 10,000 atoms with timestep $dt = 5 \times 10^{-3} \omega_p^{-1}$, for plasma frequency determined from the ionization of the 2TTCP model. The particles were thermalized in an NVT Nose-Hoover thermostat for a time of $50 \omega_p^{-1}$ before a $500 \omega_p^{-1}$ NVE production phase. Thermal conductivity and viscosity were computed from the asymptotic value of time-integrated heat-flux and pressure tensor autocorrelation functions using the corresponding Green-Kubo relations.

In Fig. 2 we compare the results of DFT-MD (black pluses) to the 2TTCP model with bridge function[33] (solid blue), MD simulation (green triangles) and find close agreement amongst the three. At LTE conditions in panel a), we have a strongly coupled aluminum plasma with average ionization $\langle Z \rangle = 3$ defined as in[10]. Around $T_e \sim 10\text{ eV}$ we start to see significant ionization until in panel d) where $\langle Z \rangle = 4.35$. The MD simulation give us confidence that the bridge function is accurate here, and we can see that our model mimics the structure of DFT-MD quite well. We additionally show the Yukawa one component plasma (YOCP) model for T_e dependent $\langle Z \rangle$ from the More Thomas-Fermi ionization fit in[44] and Thomas-Fermi screening length and the one component plasma (OCP) model. The OCP and YOCP curves are obtained from HNC with bridge functions [34] and [35], respectively. The YOCP model that the IYVM model is based on only very approximately takes into account the electronic structure.

B. Transport Coefficients

The transport properties of plasmas can depend strongly on both electron and ion temperature. In Fig. 3 we see the viscosity of aluminum depends strongly on both ionic and electronic temperatures, and deviations from LTE can result in orders of magnitude of deviation from the expected answer. This model is based on fits to MD [26, 27]

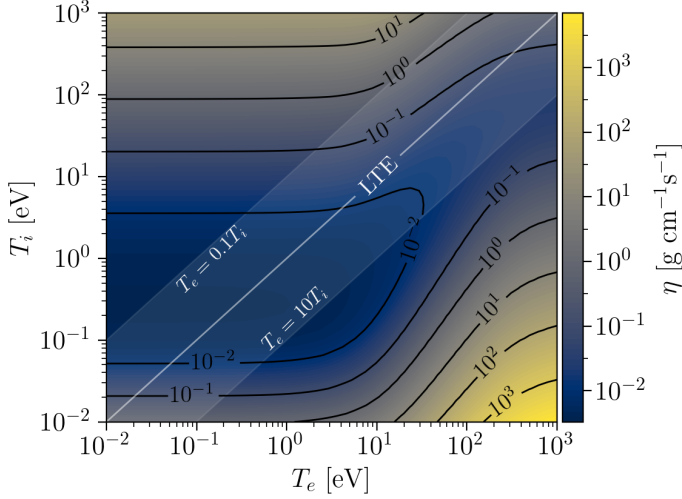


FIG. 3. The viscosity of 2.7 g/cm^3 aluminum from the improved Yukawa viscosity model in [27], which is refitted from [26] to better match high temperature scaling.

that incorporate electron temperature only through a linear Thomas-Fermi screening length, and ion temperature through pair-potential MD. In the cold electron limit, the Thomas-Fermi screening length involved depends only the Fermi energy and not T_e , so only T_I impacts viscosity until $T_e \sim \text{few eV}$. As the plasma heats, variations in the pair potential from electron heating substantially affects the resulting viscosity.

In Fig. 4 we show the ion self-diffusion coefficient computed using PPMD (squares with error bars) mean square displacements[31] as a function of electron temperature over three different ion temperatures. Error bars here and for other transport coefficients generated in this papers are defined as the standard deviation between 10 parallel runs of the time-integrated correlation functions through the Green-Kubo relations. Increasing electronic temperature ionizes electrons above about 10 eV. The ion charge then increases and the cross section increases, lowering the mean free path and D . For the $T_I = 1 \text{ eV}$ case, we ran two-temperature DFT-MD simulations, both for an eleven electron pseudopotential with VASP (triangles), and a three electron pseudopotential (pluses) with QuantumESPRESSO (QE) [28, 46], computing the self-diffusion coefficient from mean square displacement. We find very close agreement as expected from the close agreement of the pair correlations in Fig. 2. Initial DFT-MD runs were conducted with QE with a three valence electron pseudopotential (3e), which is inadequate for Aluminum above 10 eV, though we can see good agreement for lower T. For each of the ion temperatures, we have equilibrium results to compare to from

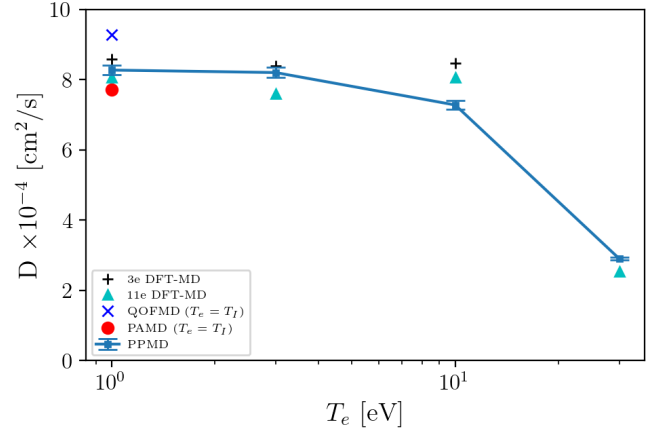


FIG. 4. Aluminum self diffusion at 2.7 g/cm^3 for varying electron temperature at $T_I = 1 \text{ eV}$ extracted from our PPMD simulations (squares with error bars), our DFT-MD MD runs (triangle), and an AA model from [19] (diamonds). The QOFMD (blue cross) and PAMD (red circle) datasets are equilibrium computations from [45].

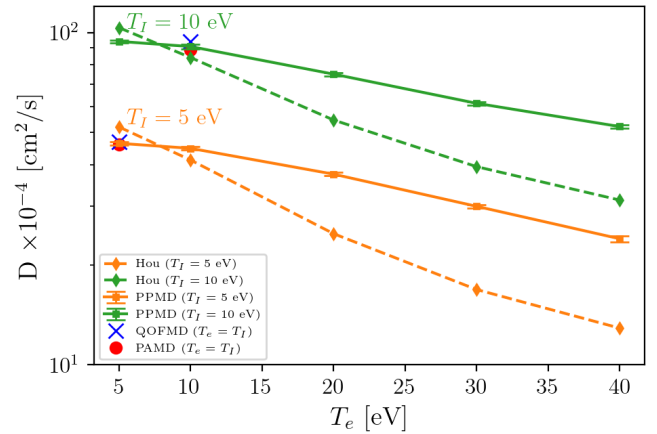


FIG. 5. Aluminum self diffusion at 2.7 g/cm^3 for varying electron temperature at two different ion temperatures, 5 eV (orange) and 10 eV (green) extracted from our PPMD simulations (squares with error bars), our DFT-MD MD runs (triangle), and an AA model from [19] (diamonds). The QOFMD (blue crosses) and PAMD (red circle) datasets are equilibrium computations from [45].

pseudo atom molecular dynamics (PAMD) and orbital free MD (QOFMD) [45]. We did not plot a main result of that paper, the effective potential (EPT) result simply because it overlaps the other two so closely.

The only other two-temperature computation of self-diffusion to the authors knowledge is in [19], which are shown in Fig. 5. The AA model(diamonds) considered by Hou et al. in that paper offers an alternative two-temperature AA scheme, based on a Gordon-Kim method for generating pair potentials[18, 47]. This method involves a sum of overlapping atomic electron clouds and would argue more approximately handles the free electron distri-

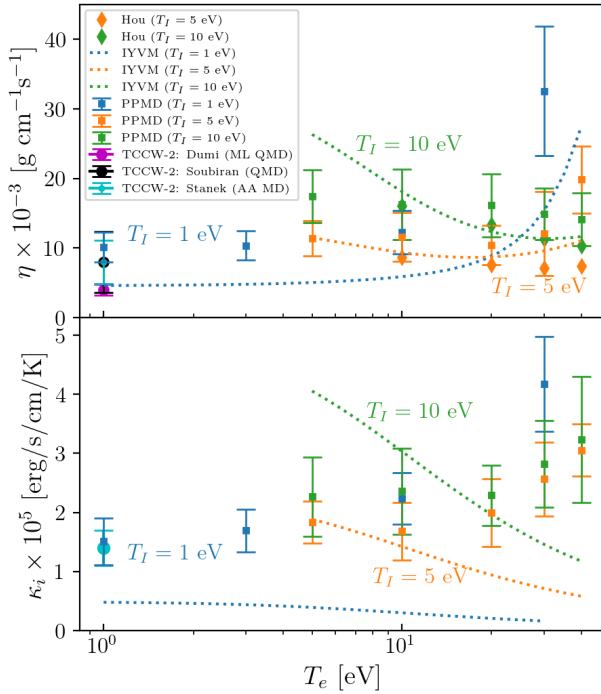


FIG. 6. **Upper**) Aluminum ion viscosity at 2.7 g/cm^3 for varying electron temperature at three different ion temperatures, 1 eV (blue), 5 eV (orange), 10 eV (green) extracted from our PPMD simulations (crosses, solid lines), compared with Hou et al. [19] (diamonds, dashed lines), and equilibrium results from the TCCW2 workshop [15] (error bars). **Lower**) Aluminum ion thermal conductivity for the same conditions.

bution as a function of ion separation than our Ornstein-Zernike based theory. Indeed we see better agreement with the results of [45], though the difference is only around 10%. Additionally, our model would predict that for $T_e \lesssim 10 \text{ eV}$, the ion-ion pair potential doesn't significantly change and thus neither does any ionic transport property, whereas Hou et al. data changes significantly in this range, which was also seen for the equation of state examined in [47]. As we move to hotter electron temperatures, away from the equilibrium case, we also see increased deviation between our PPMD result and that of Hou et al.

We also compute viscosity in the same electron and ion temperature ranges, shown in the upper panel of Fig. 6. We again compare our PPMD result to Hou et al. finding rough agreement, but a complicated temperature dependencies. The largest difference is in the highest electron temperature limit, moving far away from the dark blue viscosity minimum in Fig. 3. The reason for the increased complexity of the viscosity compared to self-diffusion is that we care about much more than just mean free paths, and instead the potential interactions of nearby ions, a strong function of T_e through $\langle Z \rangle$, is of crucial importance to the stress autocorrelation function. In the range of electron and ion temperatures shown, the total variation in viscosity ap-

pears of similar magnitude to the variation in uncertainty of the equilibrium viscosity results reported in the second transport coefficient comparison workshop (TCCW2) particles [15]. These results include an AA based PPMD (cyan) as well as two direct high fidelity DFT-MD computations.

We finally compute ionic thermal conductivity, in the lower panel of Fig. 6 using the heat flux autocorrelation function [31]. Less data is available in the literature, because the electron thermal conductivity is typically dominant. However, it is worth noting the electronic thermal conductivity scales roughly as $T_e^{5/2}$, meaning a non-equilibrium scenario where for example $T_I \gg T_e$, such as occurs in shocks [48] and ICF hotspots, could cause ion thermal conductivity to be of equal or greater importance. In this case, we note the best on-the-fly model available is SMT (dotted lines) [25], but the dependence on a binary-collision assumption can lead to qualitative disagreement in the strong coupling regime, as we see here. Our 2TTCP model coupled to PPMD is precisely the rapid computational tool needed for future exploration or fits.

IV. DISCUSSION

The multi-temperature quantum Ornstein-Zernike equations we have derived, and the accompanying average atom based two-temperature two-component plasma model have been shown to accurately generalize the equilibrium answers. Since we rely on statistical mechanical techniques, albeit generalized to multiple temperatures, there are some clear limits to this calculation. One is dynamical electron effects, since we work in the $m_e \ll m_i$ adiabatic picture, it is difficult to connect to key experimental outputs such as $S(k, \omega)$ for either electron or ion components. It is also clear that the resulting momenta distributions inherent in our model are those of a perfectly equilibrated plasma. In reality, the transient non-equilibrium system and velocity dependent cross sections would create distributions with distinct non-equilibrium distortions, whose effect on transport and EOS is not analyzed here.

This model ignores the possibility of a non-trivial cross-species temperature, such as in [49]. For electron-ion systems, this effect is vanishingly small unless the ion temperature is orders of magnitude higher than the electron temperature, for which the Born-Oppenheimer approximation would be poor regardless. For similar mass multi-temperature ion-ion or electron-positron systems, corrections might become important.

In this work we focused on modeling ionic structure and transport in the two-temperature limit. The 2TTCP model also offers an opportunity to model multi-temperature effects on electronic transport coefficients and equation of state properties for out of equilibrium plasmas. In this case, it is possible that resolving fully the effects of ions on primarily electron physics based properties might additionally require incorporating self-consistency such as going beyond Eq. (48). We leave this for future work.

- [1] M. M. Marinak, G. D. Kerbel, N. A. Gentile, O. Jones, D. Munro, S. Pollaine, T. R. Dittrich, and S. W. Haan, Three-dimensional hydra simulations of national ignition facility targets, *Physics of Plasmas* **8**, 2275 (2001).
- [2] B. Fryxell, K. Olson, P. Ricker, F. X. Timmes, M. Zingale, D. Q. Lamb, P. MacNeice, R. Rosner, J. W. Truran, and H. Tufo, Flash: An adaptive mesh hydrodynamics code for modeling astrophysical thermonuclear flashes, *The Astrophysical Journal Supplement Series* **131**, 273 (2000).
- [3] C. Orban, M. Fatenejad, S. Chawla, S. C. Wilks, and D. Q. Lamb, A radiation-hydrodynamics code comparison for laser-produced plasmas: Flash versus hydra and the results of validation experiments, arXiv preprint arXiv:1306.1584 (2013).
- [4] L. B. Fletcher, J. Vorberger, W. Schumaker, C. Ruyer, S. Goede, E. Galtier, U. Zastra, E. P. Alves, S. D. Baalrud, R. A. Baggott, B. Barbrel, Z. Chen, T. Döppner, M. Gauthier, E. Granados, J. B. Kim, D. Kraus, H. J. Lee, M. J. MacDonald, R. Mishra, A. Pelka, A. Ravasio, C. Roedel, A. R. Fry, R. Redmer, F. Fiuza, D. O. Gericke, and S. H. Glenzer, Electron-ion temperature relaxation in warm dense hydrogen observed with picosecond resolved x-ray scattering, *Frontiers in Physics* **10**, 838524 (2022).
- [5] N. Jourdain, L. Lecherbourg, V. Recoules, P. Renaudin, and F. Dorchie, Ultrafast thermal melting in nonequilibrium warm dense copper, *Phys. Rev. Lett.* **126**, 065001 (2021).
- [6] S. Mazevet, J. Clérouin, V. Recoules, P. M. Anglade, and G. Zerah, Ab-initio simulations of the optical properties of warm dense gold, *Phys. Rev. Lett.* **95**, 085002 (2005).
- [7] Z. Lin, L. V. Zhigilei, and V. Celli, Electron-phonon coupling and electron heat capacity of metals under conditions of strong electron-phonon nonequilibrium, *Phys. Rev. B* **77**, 075133 (2008).
- [8] B. Wilson, V. Sonnad, P. Sterne, and W. Isaacs, Purgatorio - a new implementation of the inferno algorithm, *Journal of Quantitative Spectroscopy and Radiative Transfer* **99**, 658 (2006).
- [9] C. E. Starrett, N. M. Gill, T. Sjoström, and C. W. Greeff, Wide ranging equation of state with tartarus: A hybrid green's function/orbital based average atom code, *Computer Physics Communications* **235**, 50 (2019).
- [10] C. E. Starrett and D. Saumon, A simple method for determining the ionic structure of warm dense matter, *High Energy Density Physics* **10**, 35 (2014).
- [11] J. Chihara, Average atom model based on quantum hypernetted chain method, *High Energy Density Physics* **19**, 38 (2015).
- [12] T. J. Callow, D. Kotik, E. Kraisler, and A. Cangi, atomec: An open-source average-atom python code, arXiv preprint arXiv:2206.01074 (2022).
- [13] R. Piron and T. Blenski, Variational-average-atom-in-quantum-plasmas (vaaqp) code and virial theorem: Equation-of-state and shock-hugoniot calculations for warm dense al, fe, cu, and pb, *Phys. Rev. E* **83**, 026403 (2011).
- [14] P. E. Grabowski, S. B. Hansen, M. S. Murillo, L. G. Stanton, F. R. Graziani, A. B. Zylstra, S. D. Baalrud, P. Arnault, A. D. Baczewski, L. X. Benedict, C. Blanchard, O. Čertík, J. Clérouin, L. A. Collins, S. Copeland, A. A. Correa, J. Dai, J. Daligault, M. P. Desjarlais, M. W. Dharma-wardana, G. Faussurier, J. Haack, T. Haxhimali, A. Hayes-Sterbenz, Y. Hou, S. X. Hu, D. Jensen, G. Jungman, G. Kagan, D. Kang, J. D. Kress, Q. Ma, M. Marciante, E. Meyer, R. E. Rudd, D. Saumon, L. Shulenburger, R. L. Singleton, T. Sjoström, L. J. Stanek, C. E. Starrett, C. Ticknor, S. Valaitis, J. Venzke, and A. White, Review of the first charged-particle transport coefficient comparison workshop, *High Energy Density Physics* **37**, 100905 (2020).
- [15] L. J. Stanek, A. Kononov, S. B. Hansen, B. M. Haines, S. X. Hu, P. F. Knapp, M. S. Murillo, L. G. Stanton, H. D. Whitley, S. D. Baalrud, L. J. Babati, A. D. Baczewski, M. Bethkenhagen, A. Blanchet, R. C. Clay, K. R. Cochrane, L. A. Collins, A. Dumi, G. Faussurier, M. French, Z. A. Johnson, V. V. Karasiev, S. Kumar, M. K. Lentz, C. A. Melton, K. A. Nichols, G. M. Petrov, V. Recoules, R. Redmer, G. Röpke, M. Schörner, N. R. Shaffer, V. Sharma, L. G. Silvestri, F. Soubiran, P. Suryanarayana, M. Tacu, J. P. Townsend, and A. J. White, Review of the second charged-particle transport coefficient code comparison workshop, *Physics of Plasmas* **31**, 52104 (2024).
- [16] M. W. C. Dharma-wardana, Electron-ion and ion-ion potentials for modeling warm dense matter: Applications to laser-heated or shock-compressed al and si, *Phys. Rev. E* **86**, 036407 (2012).
- [17] M. W. C. Dharma-wardana and F. m. c. Perrot, Energy relaxation and the quasiequation of state of a dense two-temperature nonequilibrium plasma, *Phys. Rev. E* **58**, 3705 (1998).
- [18] R. G. Gordon and Y. S. Kim, Theory for the forces between closed-shell atoms and molecules, *The Journal of Chemical Physics* **56**, 3122 (1972).
- [19] Y. Hou, Y. Fu, R. Bredow, D. Kang, R. Redmer, and J. Yuan, Average-atom model for two-temperature states and ionic transport properties of aluminum in the warm dense matter regime, *High Energy Density Physics* **22**, 21 (2017).
- [20] D. B. Boercker and R. M. More, Statistical mechanics of a two-temperature, classical plasma, *Phys. Rev. A* **33**, 1859 (1986).
- [21] L. J. Stanek, R. C. Clay, M. Dharma-Wardana, M. A. Wood, K. R. Beckwith, and M. S. Murillo, Efficacy of the radial pair potential approximation for molecular dynamics simulations of dense plasmas, *Physics of Plasmas* **28** (2021).
- [22] L. Harbour, M. Dharma-Wardana, D. D. Klug, and L. J. Lewis, Equation of state, phonons, and lattice stability of ultrafast warm dense matter, *Physical Review E* **95**, 043201 (2017).
- [23] L. Harbour, G. Förster, M. Dharma-Wardana, and L. J. Lewis, Ion-ion dynamic structure factor, acoustic modes, and equation of state of two-temperature warm dense aluminum, *Physical review E* **97**, 043210 (2018).
- [24] M. Dharma-Wardana, D. Klug, L. Harbour, and L. J. Lewis, Isochoric, isobaric, and ultrafast conductivities of aluminum, lithium, and carbon in the warm dense matter regime, *Physical Review E* **96**, 053206 (2017).
- [25] L. G. Stanton and M. S. Murillo, Ionic transport in high-energy-density matter, *Phys. Rev. E* **93**, 043203 (2016).
- [26] M. S. Murillo, Viscosity estimates of liquid metals and warm dense matter using the yukawa reference system, *High Energy Density Physics* **4**, 49 (2008).
- [27] Z. A. Johnson, L. G. Silvestri, G. M. Petrov, L. G. Stanton, and M. S. Murillo, Comparison of transport models in dense plasmas, *Physics of Plasmas* **31**, 082701 (2024), <https://pubs.aip.org/aip/pop/article->

- [pdf/doi/10.1063/5.0204226/20089386/082701.1.5.0204226.pdf](https://doi.org/10.1063/5.0204226/20089386/082701.1.5.0204226.pdf).
- [28] P. Giannozzi, S. Baroni, N. Bonini, M. Calandra, R. Car, C. Cavazzoni, D. Ceresoli, G. L. Chiarotti, M. Cococcioni, I. Dabo, A. D. Corso, S. de Gironcoli, S. Fabris, G. Fratesi, R. Gebauer, U. Gerstmann, C. Gougoussis, A. Kokalj, M. Lazzeri, L. Martin-Samos, N. Marzari, F. Mauri, R. Mazzarello, S. Paolini, A. Pasquarello, L. Paulatto, C. Sbraccia, S. Scandolo, G. Sclauzero, A. P. Seitsonen, A. Smogunov, P. Umari, and R. M. Wentzcovitch, Quantum espresso: a modular and open-source software project for quantum simulations of materials, *Journal of Physics: Condensed Matter* **21**, 395502 (2009).
- [29] G. Kresse and J. Furthmüller, Efficient iterative schemes for ab initio total-energy calculations using a plane-wave basis set, *Phys. Rev. B* **54**, 11169 (1996).
- [30] X. Gonze, B. Amadon, G. Antonius, F. Arnardi, L. Baguet, J.-M. Beuken, J. Bieder, F. Bottin, J. Bouchet, E. Bousquet, N. Brouwer, F. Bruneval, G. Brunin, T. Cavignac, J.-B. Charraud, W. Chen, M. Côté, S. Cottenier, J. Denier, G. Geneste, P. Ghosez, M. Giantomassi, Y. Gillet, O. Gingras, D. R. Hamann, G. Hautier, X. He, N. Helbig, N. Holzwarth, Y. Jia, F. Jollet, W. Lafargue-Dit-Hauret, K. Lejaeghere, M. A. L. Marques, A. Martin, C. Martins, H. P. C. Miranda, F. Naccarato, K. Persson, G. Petretto, V. Planes, Y. Pouillon, S. Prokhorenko, F. Ricci, G.-M. Rignanese, A. H. Romero, M. M. Schmitt, M. Torrent, M. J. van Setten, B. V. Troeye, M. J. Verstraete, G. Zérah, and J. W. Zwanziger, The abinit project: Impact, environment and recent developments, *Comput. Phys. Commun.* **248**, 107042 (2020).
- [31] J.-P. Hansen and I. R. McDonald, *Theory of simple liquids: with applications to soft matter* (Academic press, 2013).
- [32] N. R. Shaffer and C. E. Starrett, Correlations between conduction electrons in dense plasmas, *Phys. Rev. E* **101**, 013208 (2020).
- [33] Y. Rosenfeld and N. Ashcroft, Theory of simple classical fluids: Universality in the short-range structure, *Physical Review A* **20**, 1208 (1979).
- [34] H. Iyetomi, S. Ogata, and S. Ichimaru, Bridge functions and improvement on the hypernetted-chain approximation for classical one-component plasmas, *Phys. Rev. A* **46**, 1051 (1992).
- [35] W. Daughton, M. S. Murillo, and L. Thode, Empirical bridge function for strongly coupled yukawa systems, *Phys. Rev. E* **61**, 2129 (2000).
- [36] N. R. Shaffer, S. K. Tiwari, and S. D. Baalrud, Pair correlation functions of strongly coupled twotemperature plasma, *Physics of Plasmas* **24**, 092703 (2017) (2017).
- [37] P. Seufferling, J. Vogel, and C. Toepffer, Correlations in a two-temperature plasma, *Phys. Rev. A* **40**, 323 (1989).
- [38] J. Anta and A. Louis, Probing ion-ion and electron-ion correlations in liquid metals within the quantum hypernetted chain approximation, *Physical Review B* **61**, 11400 (2000).
- [39] B. B. L. Witte, G. Röpke, P. Neumayer, M. French, P. Sperling, V. Recoules, S. H. Glenzer, and R. Redmer, Comment on “isochoric, isobaric, and ultrafast conductivities of aluminum, lithium, and carbon in the warm dense matter regime”, *Phys. Rev. E* **99**, 047201 (2019).
- [40] G. Kresse and J. Hafner, Ab initio molecular dynamics for liquid metals, *Phys. Rev. B* **47**, 558 (1993).
- [41] G. Kresse and J. Furthmüller, Efficiency of ab-initio total energy calculations for metals and semiconductors using a plane-wave basis set, *Computational Materials Science* **6**, 15 (1996).
- [42] G. Kresse and D. Joubert, From ultrasoft pseudopotentials to the projector augmented-wave method, *Phys. Rev. B* **59**, 1758 (1999).
- [43] A. P. Thompson, H. M. Aktulga, R. Berger, D. S. Bolinteanu, W. M. Brown, P. S. Crozier, P. J. in 't Veld, A. Kohlmeyer, S. G. Moore, T. D. Nguyen, R. Shan, M. J. Stevens, J. Tranchida, C. Trott, and S. J. Plimpton, LAMMPS - a flexible simulation tool for particle-based materials modeling at the atomic, meso, and continuum scales, *Computer Physics Communications* **271**, 108171 (2022).
- [44] R. More, Pressure ionization, resonances, and the continuity of bound and free states, in *Advances in atomic and molecular physics*, Vol. 21 (Elsevier, 1985) pp. 305–356.
- [45] J. Daligault, S. D. Baalrud, C. E. Starrett, D. Saumon, and T. Sjöström, Ionic transport coefficients of dense plasmas without molecular dynamics, *Phys. Rev. Lett.* **116**, 075002 (2016).
- [46] P. Giannozzi, O. Andreussi, T. Brumme, O. Bunau, M. B. Nardelli, M. Calandra, R. Car, C. Cavazzoni, D. Ceresoli, M. Cococcioni, N. Colonna, I. Carnimeo, A. D. Corso, S. de Gironcoli, P. Delugas, R. A. DiStasio, A. Ferretti, A. Floris, G. Fratesi, G. Fugallo, R. Gebauer, U. Gerstmann, F. Giustino, T. Gorni, J. Jia, M. Kawamura, H.-Y. Ko, A. Kokalj, E. Küçükbenli, M. Lazzeri, M. Marsili, N. Marzari, F. Mauri, N. L. Nguyen, H.-V. Nguyen, A. O. de-la Roza, L. Paulatto, S. Poncé, D. Rocca, R. Sabatini, B. Santra, M. Schlipf, A. P. Seitsonen, A. Smogunov, I. Timrov, T. Thonhauser, P. Umari, N. Vast, X. Wu, and S. Baroni, Advanced capabilities for materials modelling with quantum espresso, *Journal of Physics: Condensed Matter* **29**, 465901 (2017).
- [47] Y. Hou and J. Yuan, Alternative ion-ion pair-potential model applied to molecular dynamics simulations of hot and dense plasmas: Al and Fe as examples, *Phys. Rev. E* **79**, 016402 (2009).
- [48] R. P. Drake and R. P. Drake, *Introduction to high-energy-density physics* (Springer, 2006).
- [49] M. W. C. Dharma-wardana and M. S. Murillo, Pair-distribution functions of two-temperature two-mass systems: Comparison of molecular dynamics, classical-map hypernetted chain, quantum monte carlo, and kohn-sham calculations for dense hydrogen, *Phys. Rev. E* **77**, 026401 (2008).
- [50] H. Fetsch, T. E. Foster, and N. J. Fisch, Temperature separation under compression of moderately coupled plasma, *Journal of Plasma Physics* **89**, 905890510 (2023).
- [51] M. Kardar, *Statistical Physics of Particles* (Cambridge University Press, 2007).

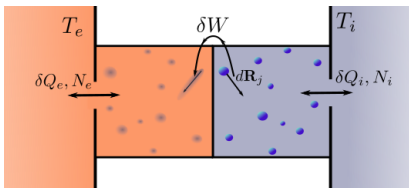


FIG. 7. Two heat reservoirs at T_e and T_I exchange heat with the electron and ion subsystems, respectively. Movement of individual ions (right) perturbs the electron subsystem (left), causing energy transfer through work δW .

Appendix A: The Two-Temperature Partition Function in the Born-Oppenheimer Approximation

Here we derive the partition function for a two-temperature system of electrons and ions, under the assumption that the electrons are inertia-less and adiabatically move to minimize their thermodynamic potential. We will arrive at an expression that is highly similar to [20].

We consider separate electron and ion subsystems, each attached to their own heat reservoir, depicted in Fig. 7. We imagine each reservoir is in the microcanonical ensemble, with the electron reservoir at temperature T_e , and the ion reservoir at T_I . Energy exchange between subsystems is allowed via work.

For the electron subsystem, the inertialess assumption implies we treat the ions as an external potential V_{ext} . Thus, the statistical mechanics of the electrons is that of the grand canonical ensemble with an external potential

$$d\Omega_e = -S_e dT_e - N_e d\mu_e + \int d^3 \mathbf{r} n_e \delta V_{\text{ext}}. \quad (\text{A1})$$

This is what is assumed in Born-Oppenheimer KSDF, and the Euler equation for this grand potential is solved for each ion MD timestep. If the electrons are in a different ensemble, the derivation can be easily adapted. The difficulty in deriving the corresponding ion statistical mechanics lies in defining precisely the effect of this electronic subsystem on the ionic one. In [50] a force balancing argument is made to derive the energy exchange of the electronic and ionic subsystems. Motivated by this, we proceed with a similar picture but in terms of ion subsystem microstates and energy exchange. First, we convert the dependence on the external potential, to an explicit dependence on the ion coordinates,

$$d\Omega_e = -S_e dT_e - N_e d\mu_e - \sum_j \mathbf{F}_j \cdot d\mathbf{R}_j, \quad (\text{A2})$$

for a force-like \mathbf{F}_j acting on each ion j from the,

$$\mathbf{F}_j = - \int d^3 \mathbf{r} n_e(\mathbf{r}) \nabla_{\mathbf{R}_j} V_{eI}(\mathbf{r}) \quad (\text{A3})$$

Assume the ions are described by a subsystem \mathcal{S}_i attached to a much larger reservoir \mathcal{R}_i in the normal thermodynamic sense[51]. The reservoir is in the microcanonical ensemble under the opposite force from the ion subsystem, means,

as usual, that it mimics the force from the electronic subsystem,

$$dU^{\mathcal{R}_i} = T_I dS^{\mathcal{R}_i} + \mu_I dN_I^{\mathcal{R}_i} - \sum_j \mathbf{F}_j \cdot d\mathbf{R}_j \quad (\text{A4})$$

Assume the ion subsystem is in a specific reference microstate μ_I^0 corresponding to a specific point in classical phase space, \mathbf{q}_I^0 , with energy E_I^0 determined by the ionic Hamiltonian $H_{II} = K_{II} + U_{II}$.

The probability of this state is determined by the number of reservoir microstates, or equivalently in terms of entropy of the bath when the microstate is in state μ_I^0 , $S_{\mathcal{R}_j}(\mu_I^0)$ as[51]

$$p(\mu_I^0) \propto e^{S_{\mathcal{R}_j}(\mu_I^0)}. \quad (\text{A5})$$

Consider then a small displacement in phase space with fixed momenta and particle number. The subsystem energy changes by dV_{II} . The entropy of the bath changes by

$$dS^{\mathcal{R}_i} = -\beta_I dV_{II} + \beta_I \sum_j \mathbf{F}_j \cdot d\mathbf{R}_j \quad (\text{A6})$$

From Eq. (A5) and Eq. (A2), we have a probability of

$$p(\mu_I^\delta) = p(\mu_I^0) \exp \left[-\beta_I \sum_j \left(\frac{\partial V_{II}}{\partial \mathbf{R}_j} + \frac{\partial \Omega_e}{\partial \mathbf{R}_j} \Big|_{T_e, \mu_e} \right) \cdot d\mathbf{R}_j \right] \quad (\text{A7})$$

We now know the probability ratio between any two points. Multiplying successive neighboring points in phase space along any path allows us to get the probability of a generic point in phase space in the form of an integral over this path. We parameterize it with λ such that at $\lambda = 0$ we have state μ_I^0 and $\{\mathbf{R}_I^0\}$, and at $\lambda = 1$ we have state μ_I^1 and $\{\mathbf{R}_I^1\}$.

$$p(\mu_I^1) \propto p(\mu_I^0) \exp \left[-\beta_I \int_0^1 d\lambda \left(\frac{\partial V_{II}}{\partial \lambda} + \frac{\partial \Omega_e}{\partial \lambda} \Big|_{T_e, \mu_e} \right) \right] \quad (\text{A8})$$

$$\propto p(\mu_I^0) \exp [-\beta_I (V_{II}^1 - V_{II}^0 + \Omega_e^1 - \Omega_e^0)] \quad (\text{A9})$$

$$\propto \exp [-\beta_I (K_{II} + V_{II} + \Omega_e)], \quad (\text{A10})$$

where in the last step we use the kinetic energy of the original state, which hasn't changed. Upon summing over ion particle number, and normalizing, we arrive at the full partition function for the two-temperature electron-ion system,

$$\Xi = \sum_{N_I} \int \prod_I \frac{d^3 \mathbf{r}_I d^3 \mathbf{p}_I}{(2\pi\hbar)^{3N_I}} e^{-\beta_I (H_I - \psi_I + \Omega_e)}, \quad (\text{A11})$$

which is related to the total free energy via

$$\Omega = -T_I \ln \Xi. \quad (\text{A12})$$

We note the resulting partition function is the same as a typical subsystem under the influence of an external force or pressure[51], but in this case acting individually on each ion. The final answer differs very slightly from Eq. (4.30) of [20] in the way in which electron number is averaged over.

Appendix B: N -Temperature Generalization

Assuming we have a hierarchy of massive particles, each of which has its own temperature. Then each level acts with the Born-Oppenheimer approximation assumed for all lower levels. Allowing for a quantum-mechanical description of each layer, we have

$$\Xi_i = \sum_{N_i} \text{Tr} e^{-\beta_i(H_i - \psi_i + \sum_{j>i}^N H_{i,j} + \Omega_{i-1})} \quad (\text{B1})$$

$$\Omega_i = -\frac{1}{\beta_i} \Xi_i \quad (\text{B2})$$

The two-temperature expectation value of an operator is defined through the partition function as,

$$\langle \mathcal{O} \rangle = \frac{1}{\Xi} \sum_{N_I, N_e} \frac{\int d^3\mathbf{r}_i d^3\mathbf{p}_i}{(2\pi\hbar)^{3N_I}} \text{Tr} [e^{-\beta_I(H_I + \psi_I) - \beta_e(H_e + \psi_e + H_{eI})} \quad (\text{B3})$$

$$\mathcal{O} e^{-(\beta_I - \beta_e)\Omega_e}]. \quad (\text{B4})$$

Then the N -temperature limit follows immediately

$$\langle \mathcal{O} \rangle = \frac{1}{\Xi} \sum_{N_{\{i\}}} \text{Tr} \left[\prod_i^N \exp[-\beta_i(H_i + \psi_i + V_i^{\text{ext}}(\{r_{j>i}\})) - \quad (\text{B5})$$

$$(\beta_{i+1} - \beta_i)\Omega_i[\{n_{j<i}\}]] \mathcal{O} \right], \quad (\text{B6})$$

where the trace is now over every species.

Appendix C: Alternative Ornstein-Zernike Formulation

The traditional form[31] of the Ornstein-Zernike does not involve a matrix inversion and is an implicit equation whose

symmetry is not obvious. However, it has some use, particular when combined with the hypernetted-chain. We start with the homogeneous Fourier space limit of Eq. (14) and combine it directly with Eq. (15),

$$\chi_{ij}(k)\chi_{0\,jj}^{-1}(k) = \delta_{ij} + \sum_k \chi^{-1}_{ik}(k)U_{kj}(k). \quad (\text{C1})$$

Where we used the fact that the ideal response function is always species-diagonal. Using the response function in terms of pair correlation functions, Eq. (33a)-(33d), and assuming ionic classical response $\chi_{0II}(k) = -\beta_I n_I$, gives the set of equations

$$\tilde{h}_{II}(k) = -\beta_I U_{II}(k) - \beta_I \sum_k n_k \tilde{h}_{Ik}(k) U_{kI}(k) \quad (\text{C2a})$$

$$-\frac{\beta_e n_e}{\chi_{0ee}(k)} \tilde{h}_{Ie}(k) = -\beta_e U_{Ie}(k) - \beta_e \sum_k n_k \tilde{h}_{Ik}(k) U_{ke}(k) \quad (\text{C2b})$$

$$\tilde{h}_{eI}(k) = -\beta_e U_{eI}(k) - \sum_k n_k \beta_k \tilde{h}_{ek}(k) U_{kI}(k) + n_e(\beta_e - \beta_I) \Delta \tilde{h}_{ee}(k) \tilde{U}_{eI}(k) \quad (\text{C2c})$$

$$-\frac{\beta_e n_e}{\chi_{0ee}(k)} \tilde{h}_{ee}(k) = n_e^{-1} (1 + \beta_e n_e \chi_{0ee}^{-1}(k)) - \beta_e U_{ee}(k) - \sum_k \beta_k n_k \tilde{h}_{ek}(k) U_{ke}(k) + (\beta_e - \beta_i) \Delta \tilde{h}_{ee}(k) n_e (\tilde{U}_{ee} - \chi_{0ee}^{-1}(k)). \quad (\text{C2d})$$

This form of the OZ equations, as opposed to Eq. (36) has useful representations of the II and Ie components for deriving the HNC equations, but with the symmetry of the correlation functions, for example eI and Ie , highly obscured.